Preprints (www.preprints.org) | NOT PEER-REVIEWED | Posted: 1 November 2021 doi:10.20944/preprints202111.0005.v1

Article

Prevention of hazards induced by a Radiation Fireball through Computational Geometry and Parametric Design

Francisco Salguero-Andújar [1], Joseph M. Cabeza-Lainez [2,*] and Federico Blasco-Macías [3]

[1] Science and Technology Research Center of Huelva, University of Huelva, Faculty of Experimental Sciences, Campus de El Carmen, 21007 Huelva, Spain; salguero@uhu.es
[2] Higher Technical School of Architecture, University of Seville, 41012 Seville, Spain
[3] Science and Technology Research Center of Huelva, University of Huelva, Faculty of Experimental Sciences, Campus de El Carmen, 21007 Huelva, Spain; federicoblasco.m@gmail.com
* Correspondence: crowley@us.es; Tel.: +34-696-749344

Abstract: Radiation Fireballs are singular phenomena which involve severe thermal radiation and consequently, they need to be duly assessed and prevented. Although the radiative heat transfer produced by a sphere is relatively well known, the shadowing measures implemented to control the fireball's devastating effects have frequently posed a difficult analytical instance, mainly due to its specific configuration. To some extent the same problem appears in volcanic explosions. In this article, since the usual solving equations for the said cases are impractical, the authors propose a novel graphic-algorithm method that sorts the problem efficiently for different kinds of obstructions and relative positions of the fireball and the defenses. Adequate application of this method may improve the safety of a significant number of facilities and persons exposed to such risks.

Keywords: prevention of explosion risks; fireball; thermal radiation of exploded combustibles; volcanic explosions; computational geometry; geometric algorithms.

1. Introduction

A Boiling Liquid Expanding Vapor Explosion (BLEVE) is a type of explosion that occurs in tanks that store liquefied and overheated gases under pressure, in which due to rupture or leakage of the tank, the liquid inside boils and is massively incorporated into the expanding vapor. The most frequent cause of this type of explosion is an external fire that engulfs the pressurized tank, weakens it mechanically, raises the temperature of the liquid contained and increases the pressure inside the tank. There comes a point in which the pressure reaches values that the container cannot withstand, producing a fissure or rupture of the same. This causes a sudden drop in pressure, the spontaneous nucleation process begins and all the liquid contained changes its state to gaseous almost instantaneously, increasing its volume hundreds or thousands of times. BLEVE occurs even though the liquid contained is not a flammable product. The combustion of the content will take place as long as the product is combustible and flammable, but this is a second explosion that constitutes a different phenomenon named as Unconfined Vapor Cloud Explosion (UVCE), also known as fireball, and is a consequence of a BLEVE and not part of it.

The formation of a fireball, isolated or as part of a BLEVE, is characterized by the emission of intense thermal radiation, capable of causing lethal and irreversible damage to people located at a significant distance. Although knowledge about this type of accident has improved substantially, they continue to occur eventually, so it is necessary to develop countermeasures aimed at reducing the effects of its consequences.

Albeit the process of formation and dynamics of fireballs, including their size, duration, elevation, temperature variation and their concentration range and velocities has been studied by numerous authors [1-7] and their initial phase is characterized by the

© 2021 by the author(s). Distributed under a Creative Commons CC BY license.

Preprints (www.preprints.org) | NOT PEER-REVIEWED | Posted: 1 November 2021 doi:10.20944/preprints202111.0005.v1

typical silhouette of a mushroom, the most widely accepted model for calculating the ensuing radiative configuration factors and their consequences is that of a sphere as a representative figure of a fireball, sometimes at ground level and sometimes elevated.

With several caveats, a similar problem appears in some volcanic explosions that require protection for visitors and researchers.

Even though it is true that there are some exact analytical calculations of configuration factors for the particular geometry of a differential element-sphere [8-13], collected mainly in the catalog of Howell and Pinar Mengüç [14], the problem of the effects and, therefore, of the calculation of the configuration factors, of a fireball partially hidden by a protection wall with an arbitrary elevation above the ground that affects an area located at any height with respect to the base-level of the fireball has been (to our best knowledge) only approached by J. M. Bonilla [15], although as the author himself recognizes (p. 97 of his doctoral thesis):

For the case that arises, a fireball with an obstacle constituted by a flat wall, the resulting integral equation is analytically unsolvable, so it is necessary to resort to numerical methods to obtain an approximate solution to the real one.

Precisely, the object of this article is to develop a parametric algorithm that provides the exact radiative configuration factors for the most general case in which the fireball is located at any distance and height above the ground, partially hidden, or not, by a protective wall over an affected area at different positions with respect to the said fireball. To this aim we would use methods based on Computational Geometry and Algorithm-Aided Design; tools that, based on the Solid Angle Projection Law, provide exact configuration factors, in all cases, even if they do not present a known analytical solution. Under such procedure, the cases with an exact analytical solution become particular results of our work.

2. Materials and Methods

2.1. Fundamental equations: Form factors and configuration factors

Since the fundamental equations governing radiant energy transfer are well established and systematically repeated in most articles dealing with radiant transfer, we will present here in short only those relationships strictly necessary for a complete understanding of our work. For a more in-depth study of the subject see for example, [16-19].

Suppose two surfaces A_i and A_j that emit diffuse radiation as shown in Figure 1. We wish to obtain the energy exchange between both surfaces. If, inititally, we ignore the details of the transmission, the problem essentially becomes one of determining the amount of energy that leaves one of the surfaces and reaches the other.

Preprints (www.preprints.org) | NOT PEER-REVIEWED | Posted: 1 November 2021 doi:10.20944/preprints202111.0005.v1

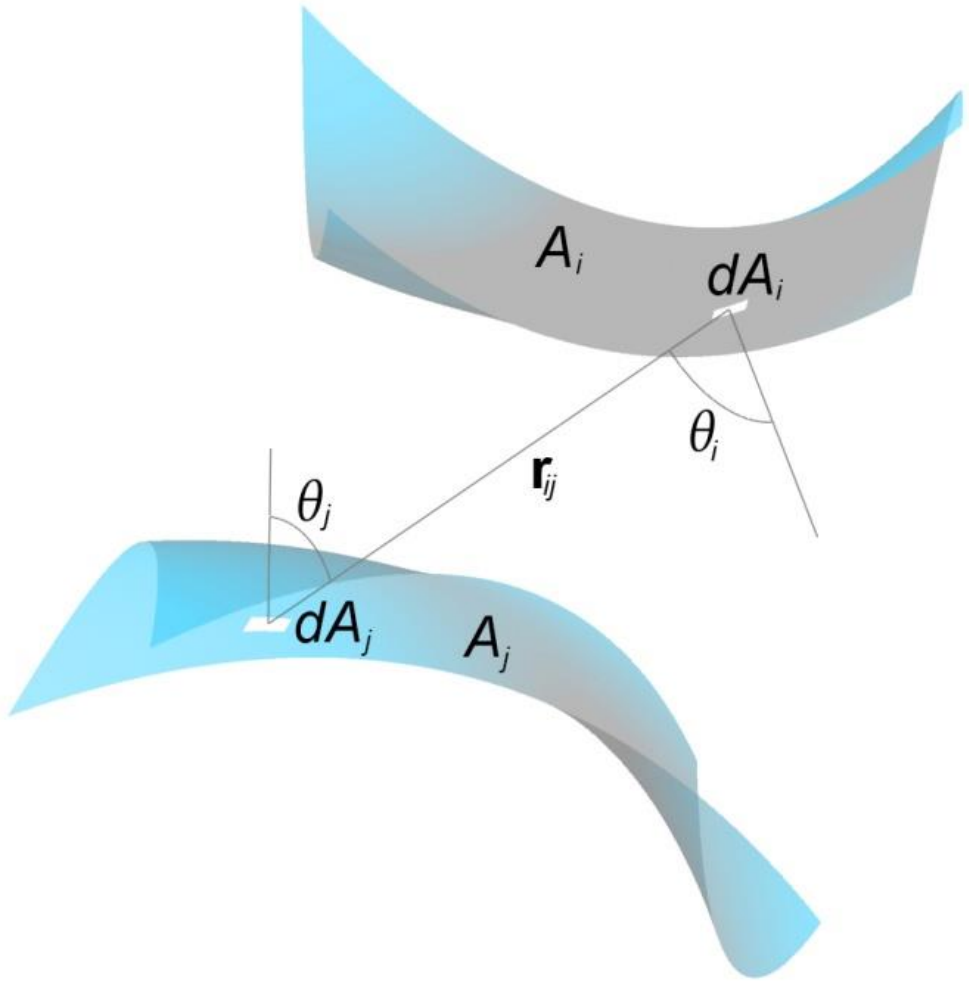

Figure 1. Arrangement of surface-source elements.

Where θ_i and θ_j represent, respectively, the angles formed by the normals to the differential elements of area dA_i and dA_j and $\mathbf{r}_{ij}$ is the vector that joins the differential surfaces dA_i and dA_j.

If we assume that there are no inter-reflections or re-emissions from one surface to the other (known as black body emission), all the incident radiation will be absorbed and the differential flux of energy will be:

$$d\phi_{ij} = (E_i - E_j)\cos\theta_i \cos\theta_j \frac{dA_i dA_j}{\pi r_{ij}^2} \quad (1)$$

Being E_i and E_j the amounts of energy (in W/m^2) emitted by surfaces i and j.

Next, let us define the *view factors* (or *form factors*), F_{ij} as the fraction of energy that radiates from surface i intercepted surface j. Then the energy that leaves the surface i and reaches the surface j will be $E_iA_iF_{ij}$ and, reciprocally $E_jA_jF_{ji}$ will be the energy that passes from the surface j to the surface i.

Then Eq. (1) could be rewritten in the form:

$$d\phi = E_iA_iF_{ij} - E_jA_jF_{ji}. \quad (2)$$

Preprints (www.preprints.org) | NOT PEER-REVIEWED | Posted: 1 November 2021 doi:10.20944/preprints202111.0005.v1

Let us now consider that there is no increase or decrease in flux and that all possible losses due to the mode of transmission are negligible, thus $d\phi = 0$, which implies that $E_iA_iF_{ij} = E_jA_jF_{ji}$, an expression known as Lambert's reciprocity theorem [20].

If we also assume (since it is a frequent case of heat transfer in UVCEs in which the energy emission of the affected surfaces is negligible) that surface A_j does not emit energy and only receives heat from A_i, the total flux will be:

$$\phi = E_i \int_{A_i} \int_{A_j} \cos\theta_i \cos\theta_j \frac{dA_i dA_j}{\pi r_{ij}^2}, \tag{3}$$

thereupon

$$E_i A_i F_{ij} = E_i \int_{A_i} \int_{A_j} \cos\theta_i \cos\theta_j \frac{dA_i dA_j}{\pi r_{ij}^2}, \tag{4}$$

and finally we get:

$$F_{ij} = \frac{1}{A_i} \int_{A_i} \int_{A_j} \cos\theta_i \cos\theta_j \frac{dA_i dA_j}{\pi r_{ij}^2}. \tag{5}$$

Which reduces the problem to the calculation of strictly geometric expressions.

However, the form factor that Eq.5 gives is the net radiant heat exchange from surface to surface. A surface that emits a certain amount of energy E_i successively induces a certain "average" energy E_2 on an adjoining surface, which tells us nothing about the detailed distribution of said energy.

When analyzing the effects of a UVCE, it is necessary to describe the flux function point by point i.e., the radiant field, and thus be able to evaluate the possible damage to people and buildings. Therefore, if we look for the point distribution of energy that reaches the surface *j*, instead of the mean, we could reduce the integral of equation (5) as A_i is concentrated on a point. The new integral will now be double, not quadruple, resulting in a new expression, also strictly geometric, known as *pointwise view factor* or *configuration factor*:

$$f_{dA_i - A_j} = \int_{A_j} \frac{\cos\theta_i \cos\theta_j}{\pi r_{ij}^2} dA_j \tag{6}$$

2.2. Nußelt's analogy or Solid Angle Proyection Law

In 1928, W. Nußelt, in an article [21] with 54 lines, 5 equations and only one figure drawn by hand, suggested that the configuration factors could be calculated graphically by 1: placing a sphere of unit radius centered on the surface element dA_1; 2: obtaining the intersection between the *cone* with its vertex in the center of said sphere and the plane surface that radiates energy (A_2) as directrix and the unit sphere; 3: projecting orthogonally the previously calculated intersection onto the plane containing dA_1 and, finally; 4: dividing by π the area enclosed by this last orthogonal projection. In this way we would obtain the configuration factor $f_{dA1\text{-}A2}$ (figure 2). Despite the short length of Nußelt's article, his intuition was taken at face value without proper demonstration and introduced the possibility of a geometric approach to a difficult analytical problem. It is convenient to stress out that Nußelt did not mention anything about non-planar emitting sources.

Preprints (www.preprints.org) | NOT PEER-REVIEWED | Posted: 1 November 2021 doi:10.20944/preprints202111.0005.v1

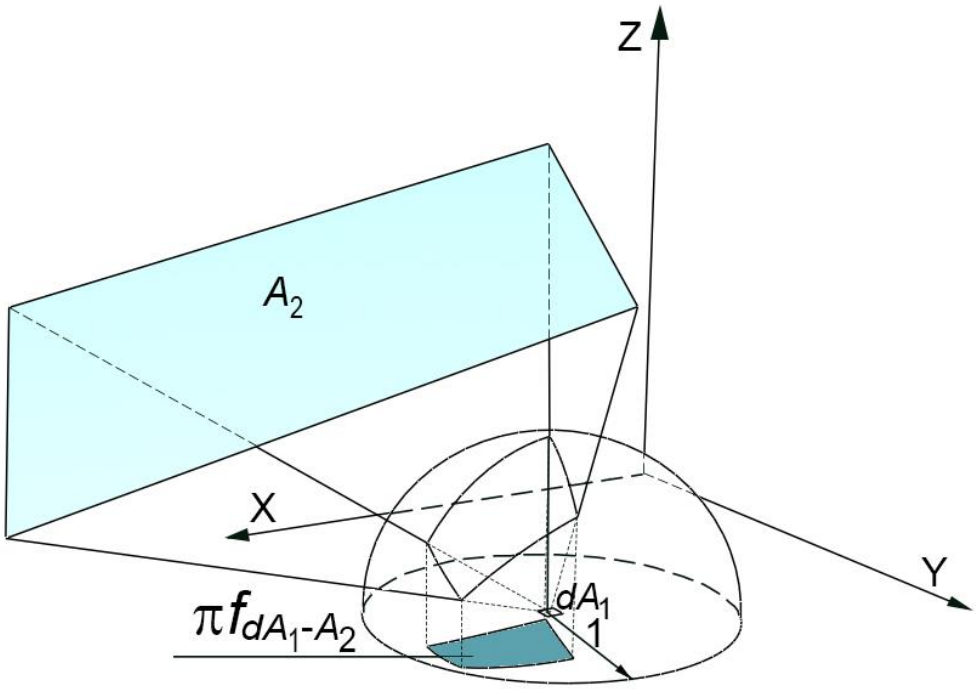

Figure 2. Nußelt's analogy.

This proposal is also known as the Solid Angle Projection Law.

Proof. Let us consider the planar surface element dA_j and join all the points of its contour with the center of a unit sphere. In this way we will obtain a conical surface with its vertex in the center of said sphere, which will delimit a $d\omega$ area on it (Figure 3). The solid angle under which a surface is seen from a point is defined as the area of the conical projection of said surface over a sphere of unit radius centered at that point.

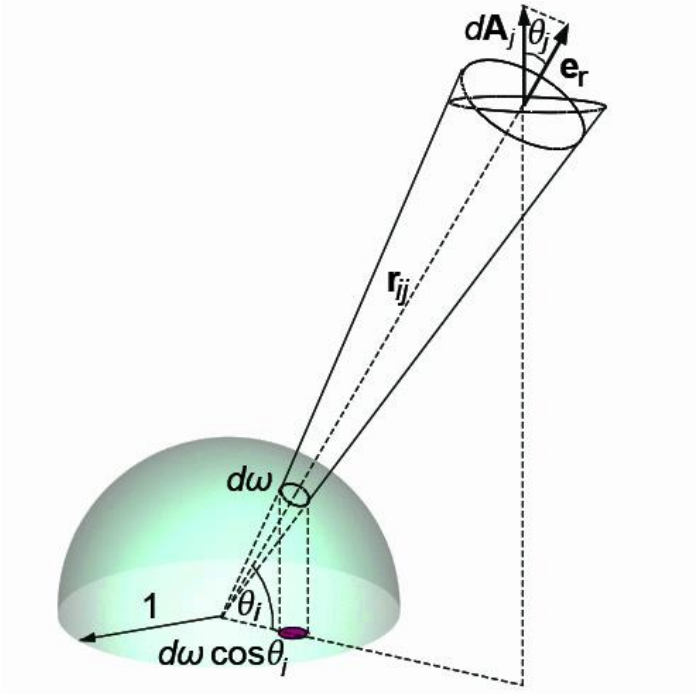

Figure 3. Solid angle $d\omega$ and its projection.

Preprints (www.preprints.org) | NOT PEER-REVIEWED | Posted: 1 November 2021 doi:10.20944/preprints202111.0005.v1

The vector $\mathbf{e}_r$ is the unit vector in the direction $\mathbf{r}_{ij}$ and the scalar product (dot product) $\mathbf{e}_r \cdot d\mathbf{A}_j = \cos\theta_j dA_j$ represents the projection of the vector $d\mathbf{A}_j$ in the radial direction $\mathbf{e}_r$, that is, $\cos\theta_i dA_j$ is the projection of the element of area dA_j over a perpendicular plane to the direction $\mathbf{e}_r$. Now, a simple similarity relation between dA_j at a distance r_{ij} and the subtended area in the unit sphere, allows us to calculate the solid angle element as:

$$d\omega = \frac{\cos\theta_j dA_j}{r_{ij}^2}. \tag{7}$$

Then the solid angle under a finite surface ω is viewed from the center of the unit sphere will be

$$\omega = \int_{A_j} \frac{\cos\theta_j}{r_{ij}^2} dA_j, \tag{8}$$

and its projection onto a plane that makes an angle θ_i with $\mathbf{e}_r$ will have a surface (with respect to the area of the circle of unit radius):

$$\frac{\omega \cos\theta_i}{\pi}, \tag{9}$$

Then substituting ω for its value we obtain:

$$\frac{\cos\theta_i}{\pi} \int_{A_j} \frac{\cos\theta_j}{r_{ij}^2} dA_j, \tag{10}$$

Since θ_i does not depend on A_j, the orthogonal projection of ω onto said plane (divided by the area of the unit circle) yields the dimensionless configuration factor previously obtained (Eq. 6):

$$f_{dA_i - A_j} = \int_{A_j} \frac{\cos\theta_i \cos\theta_j}{\pi r_{ij}^2} dA_j. \square \tag{6}$$

Furthermore, taking into account Lambert's reciprocity theorem, any surface (A_k) circumscribed by the cone under which A_j is seen, will have the same configuration factor since, as we have assumed, $d\phi = 0$ and therefore $f_{dAi\text{-}Aj} = f_{dAi\text{-}Ak}$ (Figure 4). The most important consequence of the above demonstration is that configuration factor calculation problems, no matter how complex, will always have an exact and unique solution, since the projection will have a unique value and cannot be non-existent.

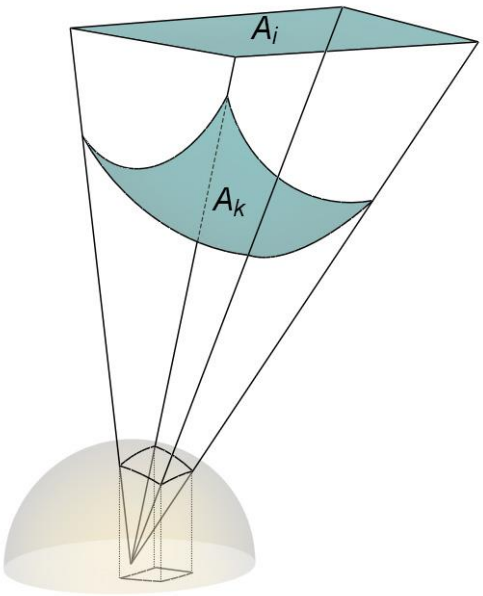

Figure 4. Equality between the configuration factors of surfaces circumscribed to the same cone.

Preprints (www.preprints.org) | NOT PEER-REVIEWED | Posted: 1 November 2021 doi:10.20944/preprints202111.0005.v1

It is important to outline that the values obtained for the configuration factors through the application of the projected solid-angle principle would not be approximations to those obtained by analytical calculations but would be identical.

However, finding a proof of the former principle by integral calculus becomes in most cases, extremely difficult. Cabeza-Lainez [19,22] has exposed this hindrance of Nußelt's work for the case of configuration factor of a rectangular emitter defined in Figure 5 (b).

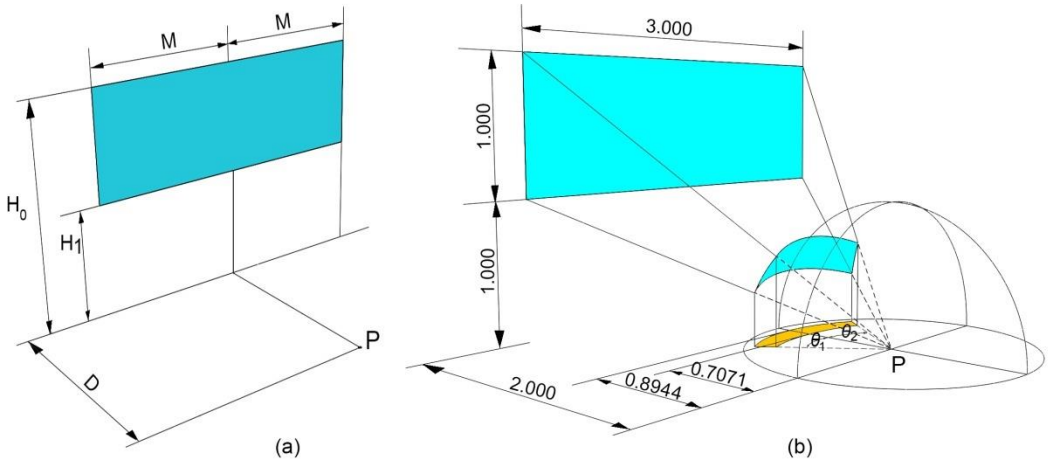

Figure 5. Solid Angle Projection Law check for a Rectangular Emitter.

The exact analytical formula obtained by direct integration of the configuration factor [22] is (Figure 5 (a)):

$$f_{12} = \frac{1}{\pi}\left[\frac{D}{\sqrt{H_1^2 + D^2}}\tan^{-1}\left(\frac{M}{\sqrt{H_1^2 + D^2}}\right) - \frac{D}{\sqrt{H_0^2 + D^2}}\tan^{-1}\left(\frac{M}{\sqrt{H_0^2 + D^2}}\right)\right], \quad (11)$$

Eq. 11 substituting the data consigned in Figure 5 (b), gives a result of:

$$f_{dA_1-A_2} = \frac{1}{\pi}\left[\frac{2}{\sqrt{5}}\tan^{-1}\left(\frac{1.5}{\sqrt{5}}\right) - \frac{2}{\sqrt{8}}\tan^{-1}\left(\frac{1.5}{\sqrt{8}}\right)\right] = 0.0584. \quad (12)$$

On the other hand, if we want to verify these values using strictly the projected solid angle principle, the only viable approach to solve the problem is to use rare generalized polar coordinates: $x = a\,\rho\cos\theta$; $y = b\,\rho\sin\theta$,

for the said coordinates, the equation of the ellipse takes the form $\rho = 1$ and the differential element of area is: $dA = ab\rho d\rho d\theta$.

Thus, to calculate the area of the elliptical sector we will have to solve:

$$A_L - A_M = \int_{\theta_2}^{\theta_1}\int_0^1 ab\rho d\rho d\theta = ab\int_{\theta_2}^{\theta_1}\left[\frac{\rho^2}{2}\right]_0^1 d\theta = ab\frac{(\theta_1 - \theta_2)}{2} = ab\theta, \quad (13)$$

since, by symmetry, $\theta_1 = -\theta_2$.

For the larger ellipse, $a = 1$ m, $b = 0.8944$ m and $\theta = \tan^{-1}(2/(1.5\cdot 0.8944)) = 0.9799$ and its complement with respect to $\pi/2$ is $(\pi/2)-\theta = \theta_L = 0.5908$, then the larger ellipse elliptical sector area is: $A_l = ab\theta_L = 1\cdot 0.8944\cdot 0.5908 = 0.5284$ m^2.

Preprints (www.preprints.org) | NOT PEER-REVIEWED | Posted: 1 November 2021 doi:10.20944/preprints202111.0005.v1

In the same way, the elliptical sector of the minor ellipse area will be, a = 1 m, b = 0.7071 m and $\theta = \tan^{-1}(2/(1.5 \cdot 0.7071)) = 1.0832$ and its complement with respect to $\pi/2$ is $(\pi/2)-\theta = \theta_M = 0.4876$ therefore $A_m = ab\theta_m = 1 \cdot 0.7071 \cdot 0.4876 = 0.3448$ m^2.

Note that the θ angles in these coordinates are different for each ellipse as they are colligated to their respective size.

Finally, subtracting the areas of the previously calculated elliptical sectors and dividing by π, we obtain exactly the same result as in eqn. (12), i. e.: $((0.5284-0.3488)/\pi) = 0.0584$.

Unfortunately, we spent five years of research to attain this finding and still other simple shapes like the circle or the ellipse remain unsolved, let alone curved emitting surface sources, as for instance the sphere. This fact convinced us of the imperious necessity of finding another approach for the issue.

2.3. Computational Geometry and Algorithm-Aided Design

Amongst the different classifications of widespread methods for the determination of configuration factors, a clear line can be traced between analytical and numerical methods, with an almost general omission of experimental methods, arising in the literature.

Although it is true that at the time that Nußelt proposed the analogy that bears his name, the available techniques lacked sufficient accuracy to develop graphic methods (so that these methods fell into disuse) currently, with the development of Computational Geometry and Algorithm-Aided Design, under programs like Grasshopper®, a recovery of the origins of graphical methods and their preferential use in a myriad of problems has been enforced [23]. We firmly believe that the solid angle principle can be applied to advantage to all kinds of non-planar sources and consequently to the problems posed by the fireball.

2.4. Calculation algorithm

The ensuing steps necessary to obtain the algorithm that gives the configuration factors of arbitrary points on differential surfaces, arbitrarily oriented and positioned, for a fireball of variable height are described below:

2.4.1. Fireball position and radius

First, we would write a simple algorithm that sets and constructs a spherical fireball of radius R (which basically depends, as we will see, of the amount and type of combustible substance) and (for convenience's sake), center at point (0,0, H_f) (Figure 6). Note that the R and H_f parameters are provided by two sliders of Grasshopper, so the radius of the fireball and its height above the soil are modifiable at will.

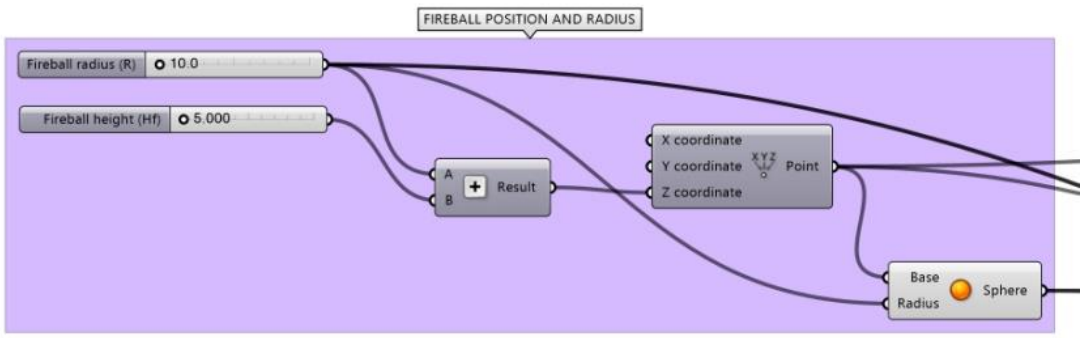

Figure 6. Initial Algorithm to represent the fireball.

The result of conducting the previous algorithm is shown in Figure 7:

Preprints (www.preprints.org) | NOT PEER-REVIEWED | Posted: 1 November 2021 doi:10.20944/preprints202111.0005.v1

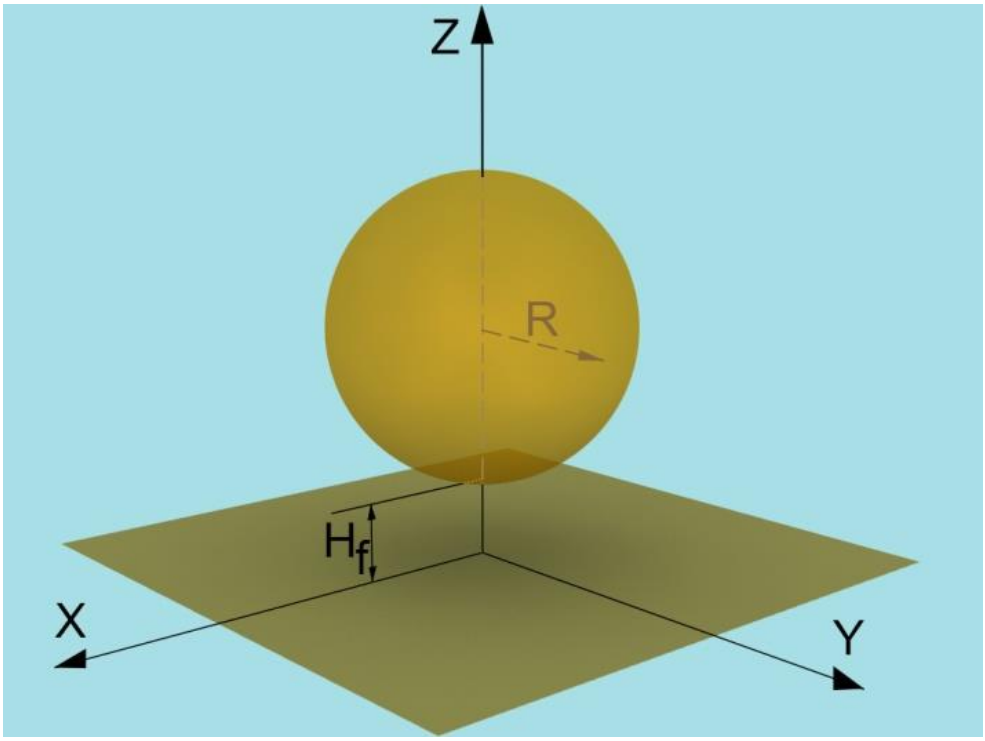

Figure 7. Fireball of radius R and height above the soil H_f.

2.4.2. Position, height, extremes of the protective wall and height of the affected area.

The second step (Figure 8), needed for the complete definition of the problem, is to set the protective wall at a certain distance from the fireball (y_w) and define its height (H_w) and its extremes. Finally, to give more generality to these types of problems, we have conceived the possibility that the fuel tanks or the vehicles that transport the combustible, could be located on a hill that overlooks the affected area by means of the H_g parameter. Again all these values are modifiable by the user depending on the specific problem to be solved. An overview of the parameters involved in this type of situation is shown in Figure 9.

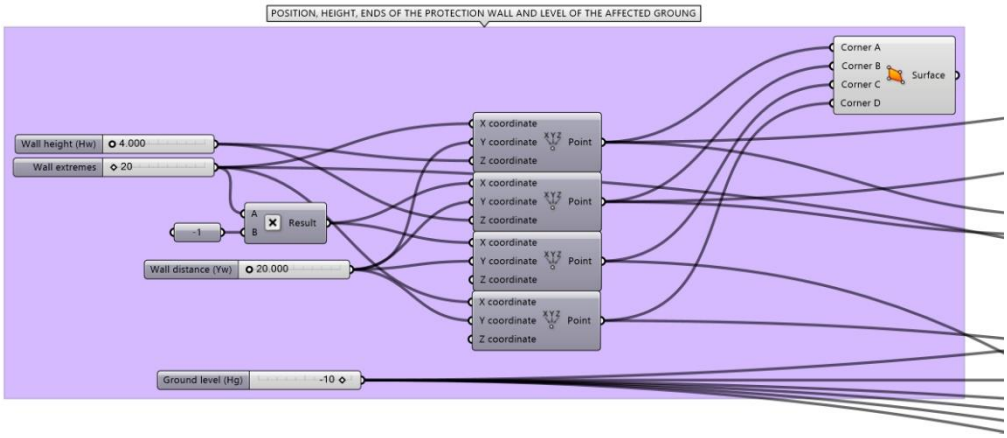

Figure 8. Other geometric parameters that define the problem in a general way.

Preprints (www.preprints.org) | NOT PEER-REVIEWED | Posted: 1 November 2021 doi:10.20944/preprints202111.0005.v1

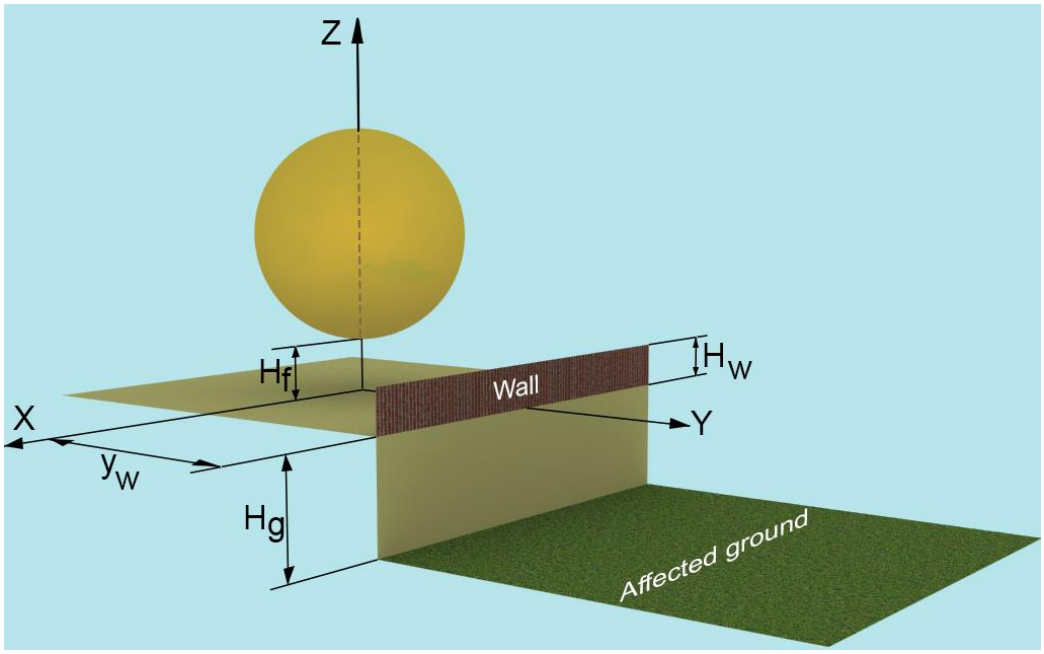

Figure 9. Graphic representation of the dependent parameters of the solution of a fireball with shadows caused by protective walls.

2.4.3. Calculation of the shadow zone provided by the protective wall.

To calculate the shadow area provided by the protective wall (Figure 10), we first calculate the intersection of the fireball with a vertical plane that passes through the center of the sphere and contains the midpoint of the highest line of the wall through the *brep|plane* function, obtaining a circumference perpendicular to the wall enclosed in the sphere.

Next, we draw the tangent lines to the said circumference from the midpoint of the upper line of the wall and select the highest of the two tangents found (*tangent lines* function). The intersection of the plane that contains the highest line of the wall and the tangent previously chosen with the ground plane (*line|plane* function), gives us the *y* coordinate of the shadow line on the exposed area, which separates the real affected zone from the area of shadow. A graphic representation of the result of the previous process is shown in Figure 11.

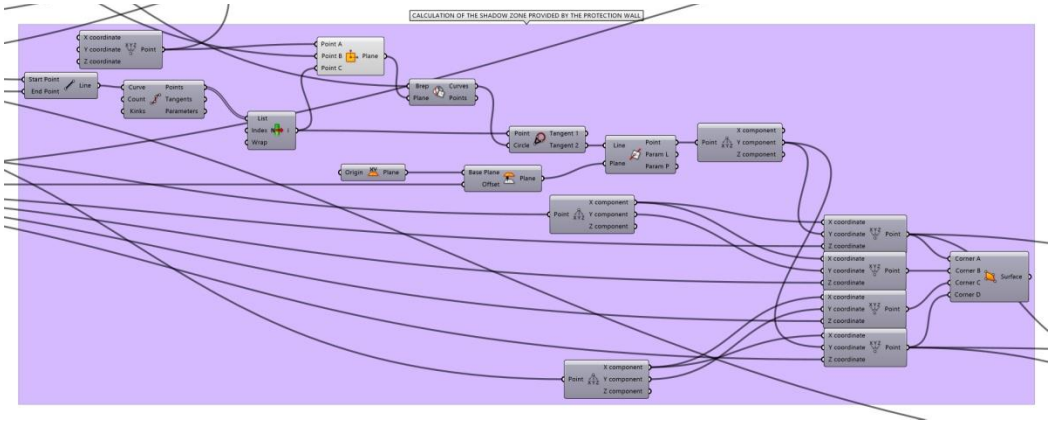

Figure 10. Calculation of the shadow zone provided by the protection wall.

Preprints (www.preprints.org) | NOT PEER-REVIEWED | Posted: 1 November 2021 doi:10.20944/preprints202111.0005.v1

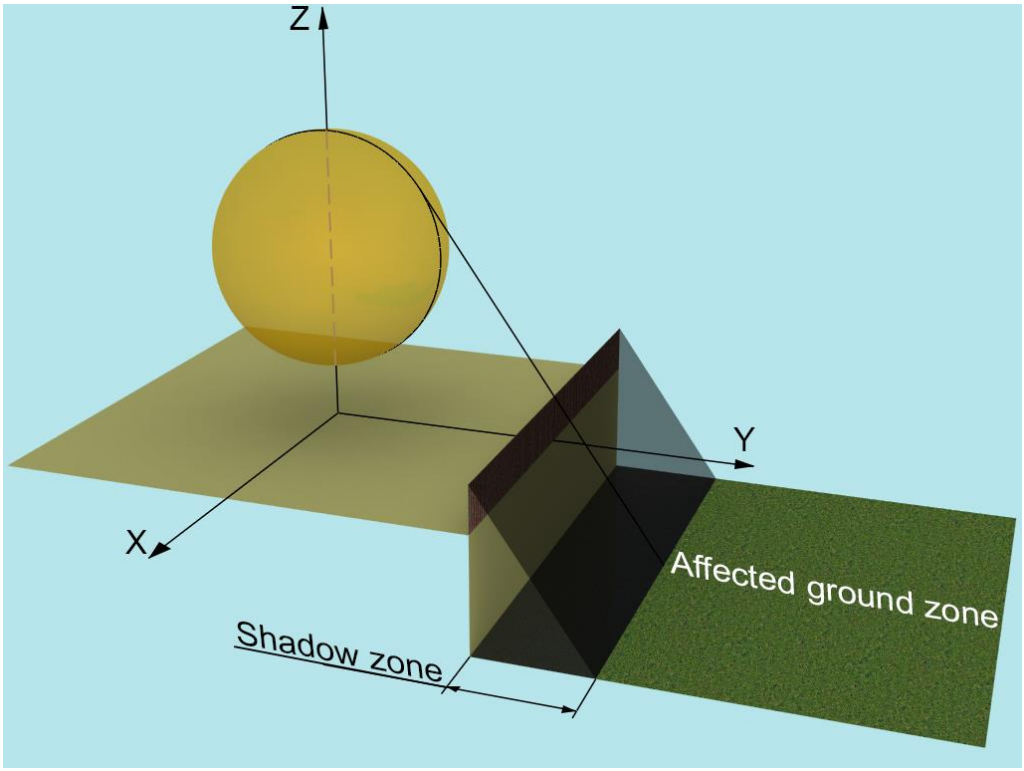

Figure 11. Shadow zone representation.

2.4.4. Create a mesh of control points to calculate configuration factors

When systematizing and automating the process, it is convenient to create a mesh of control points on which to calculate the different configuration factors between the spherical cap resulting from the section of the fireball produced by the shadow plane and that produced by the plane perpendicular to the line connecting each point to the center of the fireball. As can be seen in the algorithm depicted in Figure 12, the affected surface to be evaluated has the same width as the protection wall and its length can be modified at will by means of a slider. We also want to note that the first row of control points has been omitted, since in that entire row, the configuration factors are null by definition (Figure 13).

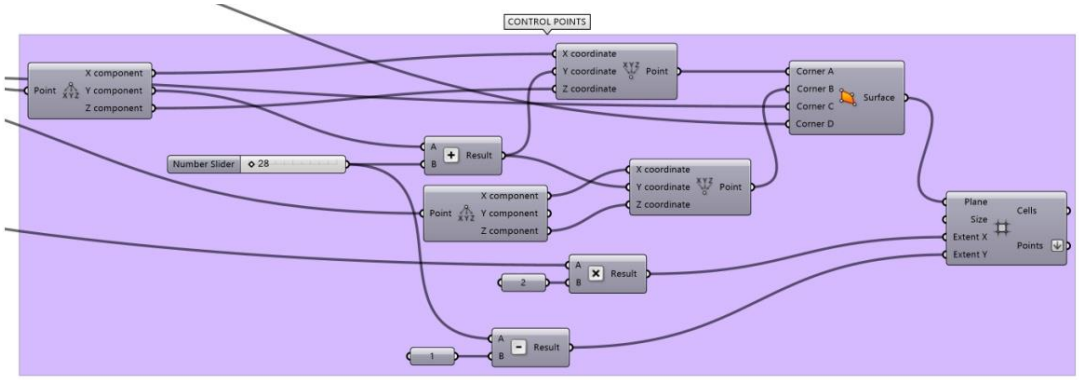

Figure 12. Algorithm to calculate an arbitrary mesh of control points.

Preprints (www.preprints.org) | NOT PEER-REVIEWED | Posted: 1 November 2021 doi:10.20944/preprints202111.0005.v1

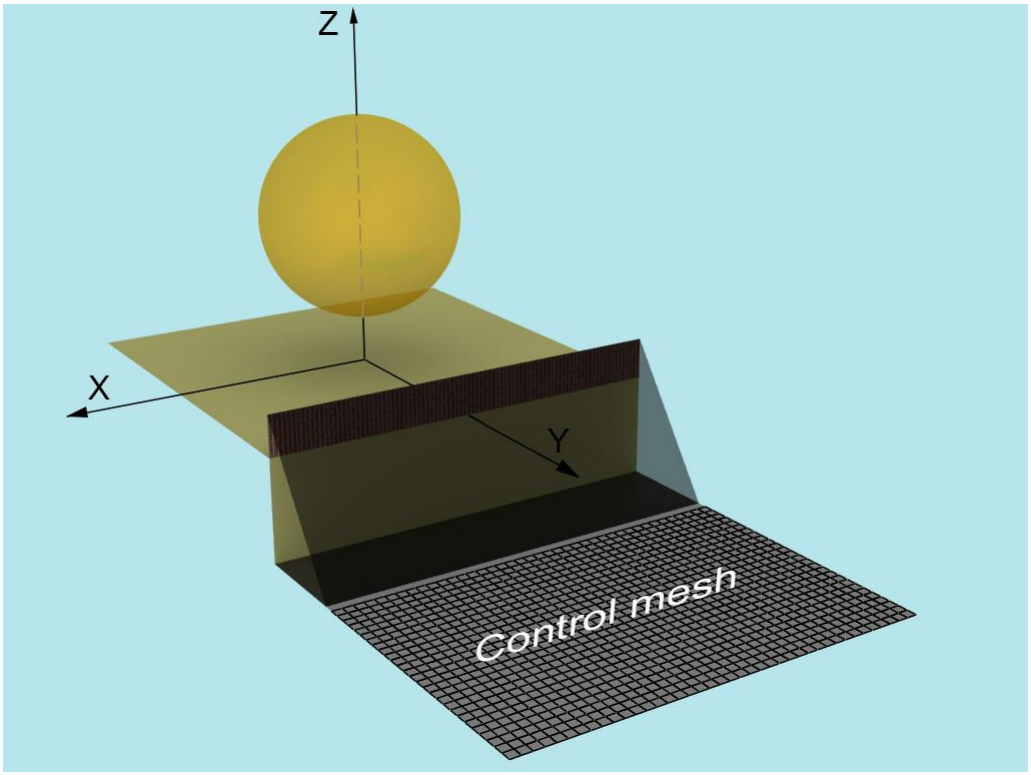

Figure 13. Control point mesh.

2.4.5. Radiant heat cones with shadow

We will now proceed to calculate the radiant heat cones with vertex at the control point tangent to the fireball, subtracting from them the part that lies below the protective wall. To perform this, given that the radiant heat cones and the fireball are two quadrics with two planes of common symmetry, one of them vertical that passes through the center of the fireball and through the control point, we would cut the fireball by the said plane to obtain a circumference contained in the fireball and in the aforementioned vertical plane. Tracing the tangents to above-defined circumference from the control points and forming the surface of revolution that generates by rotating a 2π angle, one of the previous tangents (genetratrix) around the line that joins the control point and the center of the fireball (axis), (using the *revolution* function) we obtain the complete radiant heat cone.

Next, we must cut the newly calculated cone and the fireball along the plane defined by the control point and the upper line of the protection wall (*Brep|Plane* function) by means of the *Surface Split* function, keeping the upper part of the three surfaces found by this function (Figure 14). The result is shown in Figure 15 (a).

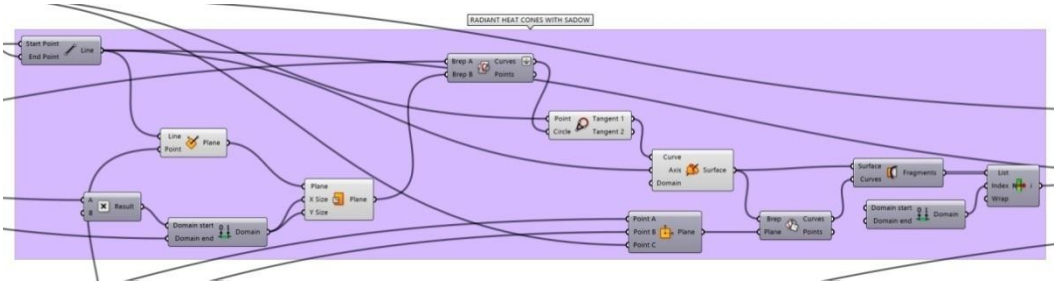

Figure 14. Algorithm for calculation the radiant heat cones with shadow.

Preprints (www.preprints.org) | NOT PEER-REVIEWED | Posted: 1 November 2021 doi:10.20944/preprints202111.0005.v1

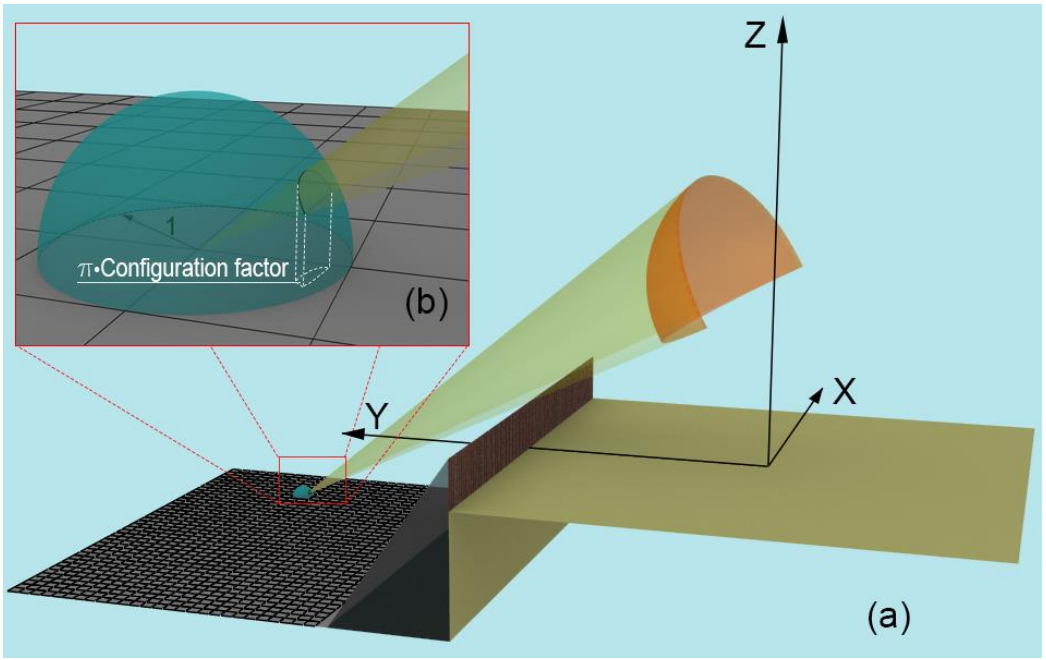

Figure 15. (a) Calculation of the radiant heat cone produced by a fireball partially behind a protective wall. **(b)** Detail of the previous figure to appreciate the application of the solid angle principle.

2.4.6. Application of the projected solid angle principle and determination of the configuration factor for an arbitrary point on the surface partially affected by a fireball

In order to achieve this, we would place a sphere of unit radius at the chosen point and obtain the intersection between the sector of the cone calculated in the previous section with the said sphere, obtaining an arc of circumference over the unit sphere (Figure 15 (b)). To close the solid angle, we need to compute the intersection circumference between the unit sphere and the plane that produced the radiating cone sector above the wall.

Of this circumference we are only interested in the smallest piece that is included between the initial and final points (*End Points*) of the intersection between the radiating cone sector and the unit sphere. To find the value of such piece, we take the midpoint of the segment that links the initial and final points and calculate the point of the unit sphere closest to it (*Curve Closest Point*). Thus, we will arrive to the arc that passes through the ends of the intersection circumference segment between the unit sphere and the radiating cone sector and its closest point.

Finally, it remains to connect the arcs previously calculated (*Join Curves*) and draw their orthogonal projection on any desired plane (vertical, horizontal or maximum exposure situation). In this case we have selected the orthogonal projection on the affected ground plane.

To complete the problem, Grasshopper calculates the area of said projection on the ground plane and divides it by π, yielding the configuration factor of the arbitrary point chosen (Figure 16):

Preprints (www.preprints.org) | NOT PEER-REVIEWED | Posted: 1 November 2021 doi:10.20944/preprints202111.0005.v1

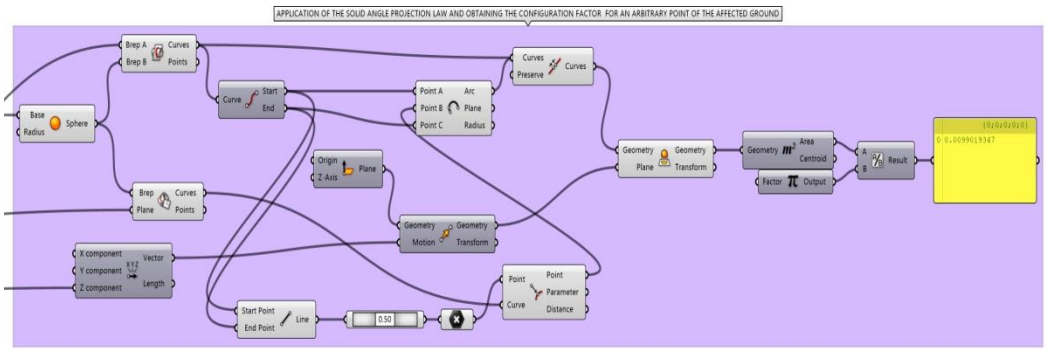

Figure 16. Application of the solid angle principle and output of the configuration factor for an arbitrary point of the affected area.

3. Results

By automating the process through a loop for all the points of the control mesh, we obtain a matrix of $n \times n$ elements that constitute every configuration factors of the affected area considered, in this case, meter by meter, although the parametric nature of the algorithm developed allows us to obtain them for any distance and plane (horizontal, vertical or maximum).

In the following example, the parameters that have been considered are:

- Fireball radius (R): 5 m.
- Fireball height (H_f): 0 m.
- Wall height: (H_w): 2 m.
- Wall distance (Y_w): 10 m.
- Ground level (H_g): 0 m.
- Horizontal affected area: 40 × 40 m: 1681 points.

Thus, we have been capable to form an innovative representation (Figure 17) of the horizontal configuration factors for a shadowed fireball, whose values are shown in Table 1.

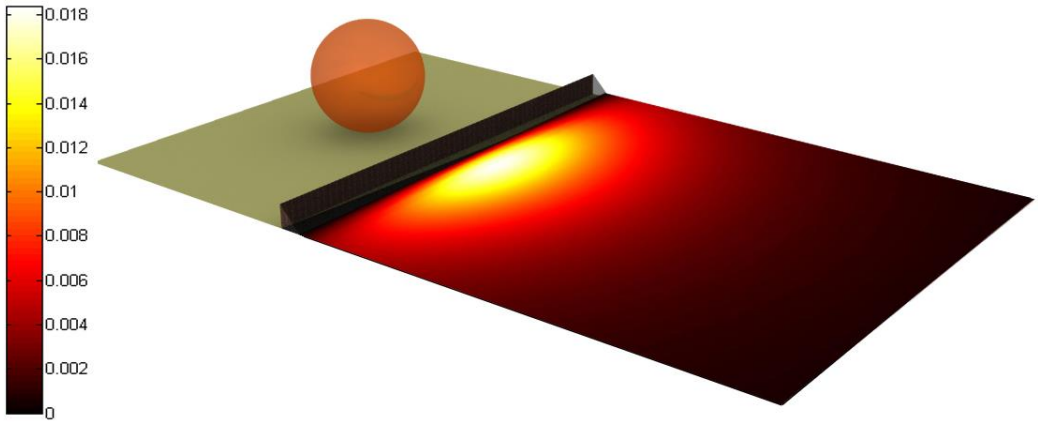

Figure 17. Newly found representation (1681 control points) of the horizontal configuration factors produced by a fireball over a 40 × 40 m² area with the following parameters: R = 5 m; H_f = 0 m; H_w = 2 m; Y_w = 10 m and Y_g = 0 m.

Preprints (www.preprints.org) | NOT PEER-REVIEWED | Posted: 1 November 2021 doi:10.20944/preprints202111.0005.v1

Table 1. Configuration factors obtained through the proposed algorithm for a fireball with the parameters described in the caption of Figure 17.

Y (m)	*X* (m)																				
	-20	-19	-18	-17	-16	-15	-14	-13	-12	-11	-10	-9	-8	-7	-6	-5	-4	-3	-2	-1	0
0	0.00000	0.00000	0.00000	0.00000	0.00000	0.00000	0.00000	0.00000	0.00000	0.00000	0.00000	0.00000	0.00000	0.00000	0.00000	0.00000	0.00000	0.00000	0.00000	0.00000	0.00000
1	0.00196	0.00218	0.00242	0.00269	0.00300	0.00335	0.00375	0.00419	0.00468	0.00523	0.00582	0.00647	0.00715	0.00786	0.00858	0.00928	0.00992	0.01047	0.01090	0.01117	0.01126
2	0.00352	0.00388	0.00429	0.00474	0.00525	0.00582	0.00645	0.00714	0.00790	0.00873	0.00962	0.01056	0.01155	0.01255	0.01354	0.01449	0.01535	0.01607	0.01663	0.01698	0.01712
3	0.00432	0.00474	0.00521	0.00573	0.00631	0.00694	0.00763	0.00839	0.00921	0.01009	0.01102	0.01200	0.01300	0.01401	0.01499	0.01591	0.01674	0.01743	0.01796	0.01829	0.01840
4	0.00466	0.00509	0.00557	0.00609	0.00666	0.00729	0.00797	0.00870	0.00949	0.01032	0.01119	0.01209	0.01300	0.01390	0.01478	0.01559	0.01631	0.01691	0.01736	0.01764	0.01774
5	0.00474	0.00516	0.00561	0.00611	0.00665	0.00723	0.00786	0.00853	0.00925	0.00999	0.01077	0.01156	0.01235	0.01313	0.01387	0.01455	0.01516	0.01565	0.01603	0.01626	0.01634
6	0.00467	0.00506	0.00549	0.00595	0.00644	0.00697	0.00754	0.00813	0.00876	0.00942	0.01009	0.01077	0.01144	0.01210	0.01272	0.01328	0.01378	0.01419	0.01449	0.01468	0.01474
7	0.00450	0.00488	0.00527	0.00569	0.00613	0.00661	0.00711	0.00763	0.00818	0.00875	0.00932	0.00990	0.01046	0.01101	0.01153	0.01199	0.01240	0.01273	0.01298	0.01313	0.01318
8	0.00433	0.00466	0.00501	0.00538	0.00578	0.00620	0.00664	0.00710	0.00757	0.00806	0.00854	0.00903	0.00951	0.00996	0.01039	0.01077	0.01111	0.01138	0.01158	0.01170	0.01174
9	0.00412	0.00441	0.00473	0.00506	0.00541	0.00579	0.00617	0.00656	0.00697	0.00739	0.00780	0.00821	0.00861	0.00899	0.00935	0.00966	0.00993	0.01015	0.01032	0.01042	0.01045
10	0.00390	0.00416	0.00444	0.00474	0.00505	0.00539	0.00571	0.00605	0.00640	0.00676	0.00711	0.00746	0.00779	0.00811	0.00840	0.00866	0.00889	0.00907	0.00920	0.00928	0.00931
11	0.00368	0.00391	0.00416	0.00443	0.00470	0.00498	0.00527	0.00557	0.00588	0.00618	0.00648	0.00677	0.00705	0.00732	0.00756	0.00778	0.00796	0.00811	0.00822	0.00829	0.00831
12	0.00346	0.00367	0.00389	0.00413	0.00437	0.00461	0.00487	0.00513	0.00540	0.00565	0.00590	0.00615	0.00639	0.00661	0.00682	0.00700	0.00715	0.00727	0.00737	0.00742	0.00744
13	0.00325	0.00344	0.00364	0.00384	0.00405	0.00427	0.00449	0.00472	0.00494	0.00517	0.00538	0.00560	0.00580	0.00598	0.00616	0.00631	0.00644	0.00654	0.00661	0.00666	0.00667
14	0.00305	0.00322	0.00339	0.00358	0.00376	0.00395	0.00415	0.00434	0.00454	0.00473	0.00492	0.00510	0.00527	0.00543	0.00557	0.00570	0.00581	0.00589	0.00595	0.00599	0.00601
15	0.00286	0.00301	0.00317	0.00333	0.00349	0.00366	0.00383	0.00400	0.00417	0.00433	0.00449	0.00465	0.00480	0.00493	0.00505	0.00516	0.00524	0.00532	0.00538	0.00548	0.00542
16	0.00268	0.00282	0.00296	0.00310	0.00325	0.00339	0.00354	0.00369	0.00383	0.00398	0.00412	0.00425	0.00437	0.00449	0.00459	0.00468	0.00476	0.00482	0.00487	0.00496	0.00490
17	0.00252	0.00264	0.00276	0.00289	0.00302	0.00315	0.00328	0.00340	0.00353	0.00366	0.00378	0.00389	0.00400	0.00410	0.00419	0.00426	0.00433	0.00438	0.00442	0.00444	0.00445
18	0.00236	0.00247	0.00258	0.00269	0.00280	0.00292	0.00303	0.00315	0.00326	0.00337	0.00347	0.00357	0.00366	0.00375	0.00382	0.00389	0.00394	0.00399	0.00402	0.00404	0.00405
19	0.00221	0.00231	0.00241	0.00251	0.00261	0.00271	0.00281	0.00291	0.00301	0.00310	0.00319	0.00328	0.00336	0.00343	0.00350	0.00356	0.00360	0.00364	0.00367	0.00369	0.00369
20	0.00208	0.00217	0.00225	0.00234	0.00243	0.00252	0.00261	0.00270	0.00278	0.00286	0.00294	0.00302	0.00309	0.00315	0.00321	0.00326	0.00330	0.00333	0.00336	0.00337	0.00338
21	0.00195	0.00203	0.00211	0.00219	0.00227	0.00235	0.00243	0.00250	0.00258	0.00265	0.00272	0.00278	0.00284	0.00290	0.00295	0.00299	0.00303	0.00306	0.00308	0.00309	0.00309
22	0.00183	0.00190	0.00197	0.00205	0.00212	0.00219	0.00226	0.00232	0.00239	0.00245	0.00251	0.00257	0.00262	0.00267	0.00272	0.00275	0.00278	0.00281	0.00283	0.00284	0.00284
23	0.00172	0.00179	0.00185	0.00191	0.00198	0.00204	0.00210	0.00216	0.00222	0.00228	0.00233	0.00238	0.00243	0.00247	0.00251	0.00254	0.00257	0.00259	0.00260	0.00261	0.00262
24	0.00162	0.00168	0.00174	0.00179	0.00185	0.00191	0.00196	0.00201	0.00207	0.00212	0.00216	0.00221	0.00225	0.00228	0.00232	0.00235	0.00237	0.00239	0.00240	0.00241	0.00241
25	0.00153	0.00158	0.00163	0.00168	0.00173	0.00178	0.00183	0.00188	0.00192	0.00197	0.00201	0.00205	0.00208	0.00212	0.00215	0.00217	0.00219	0.00221	0.00222	0.00223	0.00223
26	0.00144	0.00149	0.00153	0.00158	0.00162	0.00167	0.00171	0.00175	0.00179	0.00183	0.00187	0.00191	0.00194	0.00197	0.00199	0.00201	0.00203	0.00205	0.00206	0.00206	0.00222
27	0.00136	0.00140	0.00144	0.00148	0.00152	0.00156	0.00160	0.00164	0.00168	0.00171	0.00174	0.00177	0.00180	0.00183	0.00185	0.00187	0.00189	0.00190	0.00191	0.00191	0.00192
28	0.00128	0.00132	0.00136	0.00139	0.00143	0.00147	0.00150	0.00154	0.00157	0.00160	0.00163	0.00166	0.00168	0.00170	0.00172	0.00174	0.00175	0.00177	0.00177	0.00178	0.00178
29	0.00121	0.00124	0.00128	0.00131	0.00134	0.00138	0.00141	0.00144	0.00147	0.00150	0.00152	0.00155	0.00157	0.00159	0.00161	0.00162	0.00163	0.00164	0.00165	0.00166	0.00166
30	0.00114	0.00117	0.00120	0.00123	0.00126	0.00129	0.00132	0.00135	0.00138	0.00140	0.00142	0.00145	0.00147	0.00148	0.00150	0.00151	0.00153	0.00153	0.00154	0.00154	0.00155
31	0.00108	0.00111	0.00114	0.00116	0.00119	0.00122	0.00124	0.00127	0.00129	0.00131	0.00134	0.00135	0.00137	0.00139	0.00140	0.00142	0.00143	0.00143	0.00144	0.00144	0.00144
32	0.00102	0.00105	0.00107	0.00110	0.00112	0.00115	0.00117	0.00119	0.00121	0.00123	0.00125	0.00127	0.00129	0.00130	0.00131	0.00132	0.00133	0.00134	0.00135	0.00135	0.00135
33	0.00097	0.00099	0.00101	0.00104	0.00106	0.00108	0.00110	0.00112	0.00114	0.00116	0.00118	0.00119	0.00121	0.00122	0.00123	0.00124	0.00125	0.00126	0.00126	0.00126	0.00126
34	0.00092	0.00094	0.00096	0.00098	0.00100	0.00102	0.00104	0.00106	0.00108	0.00109	0.00111	0.00112	0.00113	0.00115	0.00116	0.00117	0.00117	0.00118	0.00118	0.00119	0.00119
35	0.00087	0.00089	0.00091	0.00093	0.00095	0.00096	0.00098	0.00100	0.00101	0.00103	0.00104	0.00106	0.00107	0.00108	0.00109	0.00110	0.00110	0.00111	0.00111	0.00111	0.00111
36	0.00083	0.00084	0.00086	0.00088	0.00090	0.00091	0.00093	0.00094	0.00096	0.00097	0.00098	0.00099	0.00101	0.00101	0.00102	0.00103	0.00104	0.00104	0.00104	0.00105	0.00105
37	0.00078	0.00080	0.00082	0.00083	0.00085	0.00086	0.00088	0.00089	0.00090	0.00092	0.00093	0.00094	0.00095	0.00096	0.00096	0.00097	0.00098	0.00098	0.00098	0.00099	0.00099
38	0.00075	0.00076	0.00078	0.00079	0.00080	0.00082	0.00083	0.00084	0.00085	0.00087	0.00088	0.00089	0.00089	0.00090	0.00091	0.00092	0.00092	0.00092	0.00093	0.00093	0.00093
39	0.00067	0.00069	0.00070	0.00071	0.00072	0.00074	0.00075	0.00076	0.00077	0.00078	0.00078	0.00079	0.00080	0.00081	0.00081	0.00082	0.00082	0.00082	0.00083	0.00083	0.00083
40	0.00064	0.00065	0.00067	0.00068	0.00069	0.00070	0.00071	0.00072	0.00073	0.00074	0.00074	0.00075	0.00076	0.00076	0.00077	0.00077	0.00078	0.00078	0.00078	0.00078	0.00078

[1] The remaining configuration factors are symmetrical to those listed in this Table. The distance Y (m) is taken from the shadow line.

3.1. Applied mathematics. Safety checks

Although the most complex issue when calculating the damage that a fireball can produce, is to obtain the configuration factors, we must not forget that it is still an issue of radiative heat transfer. Thus, we must take into account the physical parameters on which the said transfer depends to estimate the hazards that a fireball may induce on personnel present at the site. For this aim, we will require some empirical formulae proposed in the bibliography.

According to [24,25] the Thermal Radiation Dose (DTU) that produces a small probability of lethality for a average population, with second degree burns (1% lethality) is estimated at 1,000 DTU and can be calculated by the expression:

$$D_{tw} = t(I_w)^{\frac{4}{3}}, \tag{14}$$

where I_w is the intensity of the radiation in kW/m^2 and

$$t = 0.41M^{0.340} \tag{15}$$

is the time required for the fireball to reach its maximum size and M is the mass of fuel.

Preprints (www.preprints.org) | NOT PEER-REVIEWED | Posted: 1 November 2021 doi:10.20944/preprints202111.0005.v1

In turn,

$$I_w = \tau f_{max} E_p \tag{16}$$

wherein f_{max} is the maximum configuration factor at the point considered (give directly by the algorithm proposed above), and

$$\tau = 2.02\left(P_w d_f\right)^{-0.09} \tag{17}$$

is the atmospheric transmissivity, P_w is the partial pressure of vapor (typically 1,155 Pa for a 50% of relative humidity of the air) and d_f is the distance from the center of the fire-ball to the control point considered (also automatically provided by our algorithm).

On the other hand, E_p is the emissive power and is estimated by the equation:

$$E_p = \frac{\eta_{rad} M H_c}{\pi D^2 t} \tag{18}$$

where η_{rad} is the fraction of the fuel mass involved in the explosion (typically equal to 0.25). M, as we have mentioned, is the fuel mass and H_c is the calorific power of said fuel and D is provided by the equation:

$$D = 6.14 M^{0.325} \tag{19}$$

As a case study, we would suppose a tank located in an airport at ground level loaded with 40,000 liters of the most widelyused kerosene in commercial aviation, the Jet A-1, with a density of 0.8 kg / l and a calorific power H_c = 42,800 kJ / kg. We will thus have a mass of fuel M = 32,800 kg that would cause a fireball (assumed at ground level) of an estimated diameter D of = $6.14 \cdot 32{,}800^{(0.325)} \cong 179$ m.

Suppose also that a protective wall is located at 100 m from the kerosene tank and has a height of 6 m above the ground. Substituting in Eqn. (14) t and I_w by the values provided by equations (15-19) we would obtain a TDU of:

$$D_{tw} \leq 1{,}000 \leq 13.9487 \left[\frac{493.7603 f_{max}}{\left(1{,}155 d_f\right)^{0.09}}\right]^{\frac{4}{3}}, \tag{20}$$

from where we will find a safety distance with a lethality of less than 1% (D_{tw} = 996.8252 (kW / m^2) $^{4/3}$ · s) of 105.75 m measured from the protection wall, with a maximum configuration factor of f_{max} = 0.152838 at d_f = 224.17021 m.

In this manner, as the proposed algorithm is parametric, we could evaluate the distance and height of the protective wall to be built, for any given fuel mass that causes a previously established TDU.

4. Discussion and Conclusions

This article proposes and develops a new graphic algorithm, useful to calculate the configuration factors produced by a fireball of any diameter and height obstructed by a protective wall (Figure 9) in an accurate manner.

The viability of the method resides firstly, in the extension of the project solid-angle principle to non-planar emitters, as shown in subsection 2.2 and, secondly in identifying the hidden geometric features of the surfaces involved.

Our new algorithm solves the configuration factors exactly, as was previously shown. In a manner of conclusion this article presents an innovative calculation of a demanding problem that induces many casualties and economic damage per year at a worldwide scale. Besides as the thermal radiation dose received by each point of the spatial area defined is found critical aspects of the design of protections can be implemented enhancing safety and well-being of the personnel and industries concerned.

Preprints (www.preprints.org) | NOT PEER-REVIEWED | Posted: 1 November 2021 doi:10.20944/preprints202111.0005.v1

Author Contributions: Conceptualization, J.-M-C.-L.; methodology, F.S.-A.; software, F.S.-A.; validation, J.-M.C.-L., F.S.-A. and F.B.-M.; data provision, F.B.-M.; writing—original draft preparation, F.S.-A. and J.-M.C.-L.; visualization, F.S.-A. and J.-M.C.-L.; supervision, J.-M.C.-L. All authors have read and agreed to the published version of the manuscript.

Funding: This research received no external funding.

Acknowledgments: F.S.-A. would like to dedicate this work to his beloved son Enrique Salguero-Jiménez from whom he learned all he knows about Grasshopper®. J. C-L. recognizes Tomomi Odajima for strategic support and Juan Manuel Bonilla for his technical vision and contribution.

Conflicts of Interest: The authors declare no conflict of interest.

References

1. Gostintsev, Y.; Solodovnik, A.; Lazarev, V. Theory of the Aerodynamics, Self-Ignition and Burnup of Turbulent Thermals, Vortex Rings, and Jets in a Free Atmosphere. *Khim Fiz* **1982**, 9, pp. 1279-1290.
2. Prug, R.W. Quantitative Evaluation of Fireball Hazards. *Process Saf Prog* **1994**, 13, pp. 83-91.
3. Surzhikov, S.T. Thermal Radiation of Large-Scale Oxigen-Hidrogen Fireballs. Analisis of the Problem and Main Results. *Teplofiz Vysok Temp* **1997**, 35, pp. 416-423.
4. Makhviladze, G.M.; Roberts, J.P.; Yakush, S.E. Fireball During Combustion of Hydrocarbon Fuel Releases I. Structure and Lift Dynamics. *Combust Explos Shock Waves* **1999**, 35, pp. 359-369.
5. Makhviladze, G.M.; Roberts, J.P.; Yakush, S.E. Fireball During Combustion of Hydrocarbon Fuel Releases II. Thermal Radiation. *Combust Explos Shock Waves* **1999**, 35, pp. 219-229.
6. Roberts, T.; Gosse, A.; Hawksworth, S. Thermal Radiation from Fireballs on Failure of Liquefied Petroleum Gas Storage Vessels. *Process Saf Environ Prot* **2000**, 78, pp. 184-192.
7. Center for Chemical Process Safety, *Guidelines for Evaluating the Characteristics of Vapor Cloud Explosions, Flash Fires and BLEVEs. Chapter 6. Basic Principles of BLEVEs*, 2nd ed.; American Institute of Chemical Engineers: New York, NY, USA, 1994. DOI: 10.1002/9780470938157.
8. Chung, B.T.F.; Sumitra, P.S. Radiation Shape Formsfrom Plane Point Sources. *J Heat Transfer* **1972**, 94, 3, pp. 328-330. DOI: 10.1115/1.3449944.
9. Chung, B.T.F.; Naraghi, M.H.N. Some Exact Solutions for Radiation View Factors for Radiation View Factors from Spheres. *AIAA J* 1981, 19, 8, pp. 1077-1081. DOI: 10.2514/3.7843.
10. Juul, N.H. Diffuse Radiation View Factors from Differential Plane Sources to Spheres. *J Heat Tranfer* **1979**, 101, 3, pp. 558-560. DOI: 10.1115/1.3451029.
11. Hauptmann, E.G. Angle Factors Between a Small Flat Plate and a Diffusely Radiating Sphere. *AIAA J* **1968**, 6, 5, pp. 938-939. DOI: 10.2154/3.4634.
12. Naraghi, M.H. Radiative View Factors from Spherical Segments to Planar Surfaces. *J Thermophys Heat Transf* **1988**, 2, 4, pp. 373-375. DOI: 10.2514/3.56226.
13. Cabeza-Lainez, J.M.; Pulido-Arcas, J.A.; Castilla, M.-V. New Configuration Factor between a Circle, a Sphere and a Differential Area al Random Positions. J Quant Spectrosc Radiat Transf 2013, 129, pp. 272-276. DOI: 10.1016/j.jqsrt.2013.06.027.
14. Howell, J.R.; Pinar Mengüç. *A Catalog of Heat Transfer Configuration Factors*, Taylor & Francis/CRC, New York, NY, USA, 2010.
15. Bonilla, J.M. Contribución al Desarrollo de Factores de Configuración de Bolas de Fuego con Presencia de Obstáculos. PhD. Thesis. Univesitat Politècnica de Catalunya-BarcelonaTech, Barcelona, Spain, 2017.
16. Moon, P.H., *The Scientific Basis of Illumination Engineering*, Dover Publications: New York, NY, USA, 2008.
17. Modest, M.F. View Factors. In *Radiative Heat Transfer*, 3rd ed.; Academic Press: Boston, USA, 2013, pp. 129-159.
18. Howell, J.R.; Pinar Mengüç; M, Daun; K., Siegel, R., *Thermal Radiation Heat Transfer*, 7th ed.; CRC Press: Boca Raton, Florida, USA, 2020.
19. Cabeza-Lainez, J.M., *Fundamentos de Transferencia Radiante Luminosa o La Verdadera Naturaleza del Factor de Forma y sus Modelos de Cálculo*, Netbiblio: Seville, Spain, 2010.
20. Lambert, J.H. *Photometry, or, on the Measure and Gradiations of Light, Colors and Shade: Translation from the Latin of Photometria, Sive De Mensura et Gradibus Luminis, Colorum el Umbrae*, with Introductory Monograph and Notes by David L. DiLaura; Illuminating Engineering Society of North America: New York, NY, USA, 2001.
21. Nußelt, W. Graphische Bestimmung des Winkelverhältnisses bei der Wärmestrahlung. *Z Ver Dtsch Ing* **1928**, 72(20), p. 673.
22. Salguero-Andújar, F.; Cabeza-Lainez, J.-M. New Computational Geometry Methods Applied to Solve Complex Problems of Radiative Transfer. *Mathematics* **2020**, *8*, 2176.
23. Tedeschi, A. *AAD_ Algorithms-Aided Design. Parametric Strategies using Grasshopper®*, 1 st ed.; Le Penseur Publisher, Brienza, Potenza, Italy, 2014.
24. Eisenberg, N.A.; Lynch, C.J.; Breeding, R.J. *Vulnerability Model: A Simulation System for Assessing Damage Resulting from marine Spills*. Final Report. AD-A-015245. Enviro Control, Inc., Rockville, Md. USA, 1975.
25. HSE. Methods of approximation and determination of human vulnerability for offshore major accident hazard assessment 2010, pp. 1-55. https://www.hse.gov.uk/foi/internalops/hid_circs/technical_osd/spc_tech_osd_30/spctecosd30.pdf.